Organic Process Research & Development **2005**, *9*, 873–883

Control of Product Quality in Batch Crystallization of Pharmaceuticals and Fine Chemicals. Part 2: External Control

S. Rohani*

Department of Chemical and Biochemical Engineering, The University of Western Ontario, London, Ontario, Canada N6A 5B9

S. Horne and K. Murthy*

ApotexPharmaChem Inc., Station Main P.O. Box 1976, Brantford, Ontario, Canada N3T 5W5

Abstract:

We use the term "external control" to refer to two process control configurations: First, the "direct or inferential feedback control" of a given product quality index such as the crystal size distribution. Second, the "optimal control" of a process variable such as the control of the cooling policy (temperature) or the reactants addition rate to optimize an objective function defined in terms of the product quality. The intent of this two-part contribution is to discuss the various approaches used for the control of crystal quality. In Part 1, the design of the crystallization process and the selection of the process variables affecting the product quality were presented. In this part the implementation of an "external controller" will be presented. Initially, state-of-the-art instrumentation in crystallization research and technology is discussed. Mathematical models involving the population density and moments equation are presented and evaluated. Feedback control of crystal size distribution and supersaturation is presented in some detail. Polymorphic outcome of pharmaceuticals is dictated by the choice of solvent, presence of impurities, and the operating variables such as the temperature and the degree of supersaturation that are controlled by the implementation of an "external controller". A new algorithm for the solution of the integro-hyperbolic partial differential equation representing the population balance is discussed, and its potential use in the design of real-time optimal control policies for the control of batch crystallizers is highlighted. Open-loop and real-time optimal control policies in cooling batch crystallizers are presented, and their efficacy is evaluated.

I. Introduction

Efforts to implement "external control" on batch crystallizers go back to early 1970s where the sensitivity of the final crystal size distribution (CSD) to the temperature profile in a cooling batch crystallizer was investigated. It was discovered that a better CSD, i.e., a narrower size distribution and a larger mean particle size, can be ensured by using a "controlled" cooling policy as opposed to a "linear" or a "natural" cooling policy during the operation of a batch crystallizer. The pioneering work of Mullin and co-workers[1,2] and Jones[3] started a large number of publications in this area. The body of this work was primarily devoted to the cooling crystallizers. Jones[3] applied Pontryagin's maximum principle to a batch crystallizer to determine the required cooling policy. Mayrhoffer and Nyvlt[4] developed a simple cooling policy for seeded and unseeded cooling batch crystallizers.

Matthews and Rawlings[5] applied an efficient algorithm to estimate the nucleation and growth kinetics of ammonium nitrate and used this information to determine the optimal cooling policy of a batch crystallizer. Chung, Ma, and Braatz[6] and Ma, Chung, and Braatz[7] studied optimal seeding in a batch crystallizer. Recently Liotta and Sabesan[62] studied the efficacy of an ATR-FTIR for inline measurement of the supersaturation and control of the size distribution of active pharmaceutical ingredient. Christofides and co-workers, in a series of publications,[8−11] investigated the nonlinear robust control of distributed parameter systems including the particulate systems governed by the population balance equation. Rohani and co-workers in a series of communications[12−15] proposed a new numerical algorithm for the

* To whom correspondence should be addressed. E-mail: rohani@eng.uwo.ca. Telephone: (519) 661-4116. Fax: (519) 661-3498. E-mail: kmurthy@apotexpharmachem.com. Telephone: (519) 758-8942.

(1) Mullin, J. W.; Nyvlt, J. Programmed cooling of batch crystallizers. *Chem. Eng. Sci.* **1971**, *26*, 369−377.
(2) Jones, A. G.; Mullin, J. W. Programmed cooling crystallization of potassium sulphate solutions. *Chem. Eng. Sci.* **1974**, *29*, 105−118.
(3) Jones, A. G. Programmed cooling crystallization of potassium sulphate solution. *Chem. Eng. Sci.* **1974**, *29*, 105−118.
(4) Mayrhofer, B.; Nyvlt, J. Programmed cooling of batch crystallizations. *Chem. Eng. Process.* **1988**, *24*, 217−220.
(5) Matthews, H. B.; Rawlings, J. B. Batch crystallization of a photochemical: modeling, control, and filtration. *AIChE J.* **1998**, *44*, 1119−1127.
(6) Ma, D. L.; Chung, S. H.; Braatz, R. D. Optimal seeding in batch crystallization. *CJChE.* **1999**, *77*, 590−596.
(7) Ma, D. L.; Chung, S. H.; Braatz, R. D. Worst-case performance analysis of optimal batch control trajectories. *AIChE J.* **1999**, *45*, 1469−1476.
(8) Armaou, A.; Christofides, P. D. Crystal temperature control in Czochralski crystal growth process. *AIChE J.* **2001**, *47*(1), 79−106.
(9) Chiu, T.; Christofides, P. D. Nonlinear control of particulate processes. *AIChE J.* **1999**, *45*, 1279−1297.
(10) Christofides, P. D. Control of nonlinear distributed process systems: Recent developments and challenges. *AIChE J.* **2001**, *47*, 514−518.
(11) El-Farra, N. H.; Chiu, T. Y.; Christofides, P. D. Analysis and control of particulate processes with input constraints. *AIChE J.* **2001**, *47*, 1849−1865.
(12) Hu, Q.; Rohani, S.; Wang, D. X.; Jutan, A. Nonlinear Kinetic Parameter Estimation for Batch Cooling Seeded Crsytallization. *AIChE J.* **2004**, *50*, 1786−1794.
(13) Hu, Q.; Rohani, S.; Jutan, A. A new algorithm for the solution of population balance equation. *AIChE J.* **2005**. In press.

10.1021/op050050u CCC: $30.25
Published on Web 08/04/2005

solution of the population balance equation and optimal control of batch crystallizers. The algorithm was used along with the maximum likelihood method to estimate the parameter vector of nucleation and growth kinetics of ammonium sulfate−water system. The information was then used to derive and implement the optimal cooling policy to minimize the mass of the newly nucleated crystals in comparison with the seed crystals. The bulk of the reported work in this paragraph has been on the open loop optimal control of the batch crystallizers.

The major limitation of the open-loop optimal control policies is their insensitivity to batch-to-batch variations and process disturbances. In addition, to determine the optimal cooling policy, a reliable model of the crystallizer with the nucleation and growth kinetics is needed. The crystallizer model used in the above-mentioned work was either based on the population balance equation (involving an integro-partial differential equation) or the moments equations (a set of ordinary differential equations). The latter, however, does not produce an explicit representation of the crystal size distribution.

A different approach for the control of batch crystallizers is based on the direct or inferential feedback control of a major process variable such as the CSD or supersaturation. The advantage of this approach is that it is essentially a feedback control system, i.e., the controller is aware of the consequences of its action. The other advantage is that the controller does not, necessarily, require a reliable process model. Its success, however, depends on the precision and reliability of the online sensors that measure the process variables being controlled, e.g. the CSD or a property related to the CSD, or the supersaturation. For the control of CSD, measurement of fines (usually crystals smaller than 10−100 μm) suspension density and manipulation of fines dissolution rate has shown success.[16−18] Rohani and Bourne[19] simulated a batch crystallizer and used an adaptive self-tuning regulator as the feedback controller to regulate the rate of fines dissolution. A model predictive controller and a nonlinear geometric controller were also used as the feedback controller.[20−23] The direct or inferential feedback control of other properties such as supersaturation was also attempted. Redman et al.[24] used an online density meter to measure and control supersaturation. This method is, however, restricted to two-component or three-component systems and requires a careful calibration of the density meter. Recently, real-time Raman and ATR-FTIR spectroscopy have been used for the measurement of supersaturation and investigation of solvent-mediated polymorphic transformation by a few researchers including the groups of Berglund,[25] Fevotte [26,27] and Braatz.[28,29] In the area of characterization and control of crystal habit, an efficient algorithm for the determination of crystal shape based on the Fourier descriptors was suggested by Hundal et al.[30] A powerful technique based on the supervised neural network was used to classify crystals in several classes. Later, Patience and Rawlings[31] implemented an online image analyzer to control crystal habit in a batch crystallizer using an online image capturing and analysis system.

A third approach that addresses the shortcomings of the above techniques, namely insensitivity to the disturbances and batch-to-batch variability (in the case of open-loop optimal control), on one hand; and excessive reliance on accurate real-time instrumentation (in the case of feedback control), on the other hand; is the "real-time" or "online" optimal control. In this approach the optimal policy (e.g. the optimal temperature profile in a cooling crystallizer) is updated as soon as new information becomes available from the process. Schlasner et al.[32] determined the online optimal control based on the estimates of the state variables and parameters obtained from an extended Kalman filter (EKF). Rosendorf et al.[33] applied a simple online optimal control algorithm on a rectification column. Terwiesch[34] presented a cautious corrector that incorporated uncertainties of the state estimates in the online optimization of a nonisothermal batch reactor. Zhang and Rohani[35] implemented a real-time

(14) Hu, Q.; Rohani, S.; Jutan, A. Modeling and Optimization of Batch Seeded Cooling Crystallizers. *Comput. Chem. Eng.* **2005**, *29* (4), 911−918.
(15) Hu, Q.; Rohani, S.; Jutan, A. Optimal Control of a Seeded Batch Crystallizer. *Powder Technol.* **2005**. In press.
(16) Rohani, S.; Paine, K. Feedback Control of Crystal Size Distribution in a Continuous Cooling Crystallizer. *Can. J. Chem. Eng.* **1991**, *69*, 165−172.
(17) Tadayyon, A.; Rohani, S. Control of Fines Suspension Density in the Fines Loop of a KCl Crystallizer. *Can. J. Chem. Eng.* **2000**, *78*, 663−673.
(18) Rohani, S.; Tavare, N. S.; Garside, J. Control of Crystal Size Distribution in a Batch Cooling Crystallizer. *Can. J. Chem. Eng.* **1990**, *68*, 260−67.
(19) Rohani, S.; Bourne, J. R. A Simplified Approach to the Operation of a Batch Crystallizer. *Can. J. Chem. Eng.* **1990**, *68*, 799−806.
(20) Rohani, S.; Haeri, M.; Wood, H. C. Modeling and Control of a Continuous Crystallization Process, Part 1: Linear and Non-Linear Modeling. *Comput. Chem. Eng.* **1999**, *23*, 263−277.
(21) Rohani, S.; Haeri, M.; Wood, H. C. Modeling and Control of a Continuous Crystallization Process, Part 2: Model Predictive Control. *Comput. Chem. Eng.* **1999**, *23*, 279−286.
(22) Xie, W.; Rohani, S.; Phoenix, A. Extended Kalman Filter Non-Linear Geometric Control of a Seeded Batch Cooling Crystallizer. *Can. J. Chem. Eng.* **2002**, *80*, 167−173.
(23) Corriou, J. P.; Rohani, S. Non-Linear Control of a Batch Crystallizer. *Chem. Eng. Commun.* **2002**, *189*, 1415−1436.
(24) Redman, T. P.; Rohani, S.; Strathdee, G. On-line Control of Supersaturation in a Continuous Cooling KCl Crystallizer. *Can. J. Chem. Eng.* **1995**, 73.
(25) Wang, F.; Wachter, J. A.; Antosz, F. J.; Berglund, K. A. An investigation of solvent-mediated polymorphic transformation of progesterone using in situ Raman spectroscopy. *Org. Process Res. Dev.* **2000**, *4*, 391−395.
(26) Lewiner, F.; Klein, J. P.; Puel, F.; Fevotte, G. On-line ATR FTIR measurement of supersaturation during solution crystallization processes. *Chem. Eng. Sci.* **2001**, *56*, 2069−2084.
(27) Fevotte, G. New perspectives for the on-line monitoring of pharmaceutical crystallization processes using an in-situ infrared spectroscopy. *Int. J. Pharm.* **2002**, *241*, 263−278.
(28) Togkalidou, T.; Tung, H.-H.; Sun, Y.; Andrews, A.; Braatz, R. D. Solution concentration prediction for pharmaceutical crystallization processes using robust chemometrics and ATR FTIR spectroscopy. *Org. Process Res. Dev.* **2002**, *6*, 317−322.
(29) Fujiwara, M.; Chow, P. S.; Ma, D. L.; Braatz, R. D. Paracetamol crystallization using laser backscattering and ATR FTIR spectroscopy: Metastability, agglomeration and control. *Crystal Growth Des.* **2002**, *2*, 363−370.
(30) Hundal, H. S.; Rohani, S.; Wood, H. C.; Pons, M. N. Particle Shape Characterization Using Image Analysis and Neural Networks. *Powder Technol.* **1997**, *91*, 217−227.
(31) Patience, D. B.; Rawlings, J. B. Particle-shape monitoring and control in crystallization processes. *AIChE J.* **2001**, *47*, 2125−2130.
(32) Schlasner, S. M.; Strohl, W. R.; Lee, W. K. In On-line adaptive optimal control of a fed-batch fermentation of *Streptomyces* C5. *Proc. Am. Control Conf.* **1987**, *1*, 687−692.
(33) Rosendorf, P.; Kubicke, M.; Schongut, J. On-line optimization of a rectification column. *Comput. Chem. Eng.* **1988**, *12*, 199−203.
(34) Terwiesch, P. Cautious on-line correction of batch process operation. *AIChE J.* **1995**, *41*, 1337−1340.
(35) Zhang, G.; Rohani, S. On-Line Optimal Control of a Seeded Batch Crystallizer. *Chem. Eng. Sci.* **2003**, *58*, 1887−1896.

optimal controller on an ammonium sulfate-seeded cooling crystallizer. The online measurements were restricted to the crystallizer temperature and solute concentration. An extended Kalman filter was used to estimate the remaining unmeasured system states. The estimated states were used to calculate the new optimal control policy every 100 s. The calculated optimal control policy was implemented for the next 100 s, and the entire cycle was repeated using the measured and estimated states as the new initial conditions for the optimizer.

Most of the work discussed above has been restricted to the control of the CSD and supersaturation in cooling batch crystallizers. Other properties of similar or even more importance in the pharmaceutical and fine chemical industries are the product yield, purity, morphology, and polymorphic distribution. In addition to the cooling crystallization, reaction crystallization, evaporative crystallization, and drowning-out crystallization are very common. In fact in many instances in the production of active pharmaceutical ingredients (API), a combination of the various crystallization techniques is used to create the necessary supersaturation and increase the product yield.

The objective of this contribution is to review different approaches suggested in the literature for the control of batch crystallization processes and choose the most efficient algorithm. Although cases considered in this part of the contribution are restricted to the cooling crystallizers, the principles discussed are general and can be extended to the control of supersaturation in other crystallization processes. Polymorphic outcome depends on the solvent used, impurities present in the crystallization magma, and the operating conditions such as the local supersaturation and temperature. Therefore, control of supersaturation and crystallization temperature provides an effective means for the control of polymorphism. Fine-tuning and further improvement in the product quality may be achieved by implementing the "external control" either in the form of a "direct/inferential control" or in the form of an "open-loop" or "real-time" optimal control. The "design of crystallization processes" was discussed in Part 1 of this contribution. The "external control" will be explored in Part 2.

II. The External Control

Only after sufficient care is exercised in the proper design of a crystallization process by considering each point discussed in Part 1 of this contribution, an attempt should be made to implement an external controller to further improve the quality of the product. If enough attention is not paid to the preliminary design of the crystallization process, external control may never result in the desirable product with high purity, proper morphology, size distribution, and polymorphic specification. Implementation of the external control depends on reliable real-time instrumentation, accurate process models, efficient parameter and state estimation algorithms, and robust optimal controllers.

Two fundamentally different approaches have been used for the control of batch crystallizers. The traditional approach is based on the determination of the optimal cooling policy in cooling crystallizers. The advent of accurate and reliable measurement devices has recently shifted the attention to the implementation of feedback control systems. In what follows we consider the latter technique first because of is simplicity and ease of implementation. Before discussing the controller design, however, it would be beneficial to discuss modeling and parameter estimation applied to the crystallization processes and review the state-of-the-art sensor technology applied to the real-time in situ measurement of crystallization processes.

II.1. Modeling and Solution Algorithms Applied to Batch Crystallizers. In general the population balance in a batch crystallizer can be written as:[36]

$$\frac{\partial n(v,t)}{\partial t} + \frac{\partial [G(v,t)n(v,t)]}{\partial v} = B_{nuc}(v,t) + B_{agg}(v,t) - D_{agg}(v,t) + B_{br}(v,t) + D_{br}(v,t) \quad (1)$$

where $n(v,t)$ is the population density of crystals of volume v at time t, $G(v,t)$ is the growth rate of crystals of volume v, $B(v,t)$ and $D(v,t)$ represent the birth and death rate of particles of volume v, and subscripts *nuc*, *agg*, and *br* refer to nucleation, aggregation, and breakage processes, respectively. Assuming that the crystals retain their shape, there is no aggregation and breakage of the crystals, and that nucleation occurs at zero crystal size, eq 1 can be simplified to:

$$\frac{\partial n(r,t)}{\partial t} + \frac{\partial [G(r,t)n(r,t)]}{\partial r} = 0 \quad (2)$$

where r represents a characteristic crystal size. The boundary condition of eq 2 is the ratio of nucleation rate to growth rate of crystals with size zero.

$$n(0,t) = \frac{B(t)}{G(r,t)}|_{r=0} \quad (3)$$

Equation 2 has to be solved along with the mass balance and the energy balance around the crystallizer:

$$\frac{dC(t)}{dt} = -3\rho_c k_v G(r,t) m_2(t) \quad (4)$$

$$\frac{dT(t)}{dt} = -\frac{UA}{M(t)c_p}(T(t) - T_j(t)) - \frac{\Delta H_{crys}}{c_p} 3\rho_c k_v G(r,t) m_2(t) \quad (5)$$

where ρ_c is the crystal density, k_v is the volume shape factor of the crystals, UA is the product of the overall heat transfer coefficient by the heat transfer area between the crystallizer and the cooling jacket, $T(t)$ and $T_j(t)$ are the crystallizer and cooling jacket temperatures, $M(t) = \rho_c k_v m_3(t)$ is the crystal suspension density in the crystallizer expressed in terms of the third moment of the population density, and $m_2(t)$ is the second moment of the population density. The jth moment of the population density is defined in terms of the population density function by:

$$m_j(t) = \int_0^{r_{max}} r^j(t) n(r,t) dr \quad (6)$$

(36) Randolph, A. D.; Larson, M. A. *Theory of particulate processes*, 2nd ed.; Academic Press: New York, 1988.

The nucleation and size-independent growth rates are often expressed by empirical equations of the form:

$$B(t) = k_b \exp(-E_b/RT(t)) [\sigma(t)]^b \quad (7)$$

$$G(t) = k_g \exp(-E_g/RT(t)) [\sigma(t)]^g \quad (8)$$

where k_b, b, k_g, and g are the nucleation and growth rate parameters to be estimated using the experimental data. The parameter vector also includes E_b and E_g that are the nucleation and growth rate activation energies, respectively. R is the universal gas constant, and $\sigma(t)$ is the supersaturation defined in terms of a concentration difference ratio defined as:

$$\sigma(t) = \frac{C(t) - C^*(t)}{C^*(t)} \quad (9)$$

where $C^*(t)$ is the equilibrium solute concentration at any given temperature and time. The supersaturation for organic compounds is defined in terms of the activity of the solute molecules.

Solution of the above equations renders the evolution of the solute concentration, crystallizer temperature, and the crystal size distribution (CSD) with time. Solution of eq 2, which is a hyperbolic partial differential equation along with eqs 4 and 5 that are ordinary differential equations, is often a formidable task. Hu et al.[12,13] have offered a solution methodology that converts eq 2 to a set of algebraic equations that can easily be solved with the finite difference approximation of eqs 4 and 5. The method is fairly general and can be used in the presence of crystal aggregation and breakage. The reader is referred to ref 13 for the details of the solution methodology. In the absence of nucleation, aggregation, and breakage, the population densities at t_1 and t_2 are related by:

$$n(r_1,t_1)\Delta r_1 = n(r_2,t_1 + \Delta t_1)\Delta r_2 \quad (10)$$

This leads to an algebraic equation for the evaluation of the population density of crystals with size r_2 at time $t_1 + \Delta t_1$ in terms of the population density of crystals with size r_1 and at time t_1:

$$n(r_2,t_1 + \Delta t_1) \approx \frac{n(r_1,t_1)}{1 + \frac{\partial G(r,t_1)}{\partial r}|_{r=r_1}} \quad (11)$$

Note that, for a size-independent growth rate and in the absence of aggregation and breakage, eq 11 correctly anticipates that the population balance remains unchanged, and the crystals simply grow to larger sizes and the population density shifts along the crystal size axis.

An alternative modeling approach that does not render the crystal size distribution explicitly, is the moments equation. Multiplying eq 2 by r^j and integrating over the entire size range and assuming a size-independent growth rate, results in the moments equation:

$$\frac{dm_j(t)}{dt} = 0^j + jG(t)m_{j-1}(t) \quad (12)$$

To avoid solving a partial differential equation, many investigators have used the moments equation along with the solute and energy balance. In terms of the moments equation, the mathematical model of a batch crystallizer including mass and energy balance can be written in a compact form in the state space formulation:

$$\dot{x} = \frac{dx(t)}{dt} = f(x) \quad (13)$$

where

$$x^T(t) = [x_1(t)\cdots x_8(t)]$$
$$= [m_0(t)\cdots m_5(t)C(t)T(t)] \quad (14)$$

$$f(x) = \begin{bmatrix} f_1(x) \\ \vdots \\ f_8(x) \end{bmatrix} = \begin{bmatrix} B(t) \\ x_1(t)\, G(t) \\ 2x_2(t)\, G(t) \\ 3x_3(t)\, G(t) \\ 4x_4(t)\, G(t) \\ 5x_5(t)\, G(t) \\ -\,3\rho_c k_v G(t)\, x_4(t) \\ -\frac{UA}{\rho_c k_v c_p x_4(t)}(x_8(t) - T_j(t)) - \frac{\Delta H_{crys}}{c_p} 3\rho_c k_v G(t) x_3(t) \end{bmatrix} \quad (15)$$

where $[x_1(t)\cdots x_8(t)]$ are the system states, and superscript ^{T} represents transpose of a vector. Note that eq 13 is a set of ordinary differential equations that can easily be solved with standard numerical methods. Instead of the entire CSD, however, this equation only provides the average crystal size, $\bar{r}(t)$, and the coefficient of variation, CV, of the size distribution given by, for example:

$$\bar{r}(t) = \frac{m_4(t)}{m_3(t)} \quad \text{and} \quad CV = \sqrt{\frac{m_3(t)\, m_5(t)}{[m_4(t)]^2} - 1} \quad (16)$$

II.2. Parameters Estimation for Nucleation and Growth Rates. Estimation of the secondary nucleation rate and growth rate from a mixed-suspension, mixed-product removal, continuous crystallizer was suggested by Randolph and Larson.[36] Ever since, many investigators have adopted different techniques to extract nucleation and growth kinetics using the experimental data from either a batch or a continuous crystallizer. Dash and Rohani[37] suggested an iterative parameter estimation technique to determine the crystallization kinetics in a batch crystallizer by minimizing the sum of the squares of errors between the measured and the calculated final CSD. Miller and Rawlings[38] used an efficient parameter estimation method to identify a batch crystallizer. Hu et al.[12] used a nonlinear maximum likelihood algorithm to estimate the parameter vector that included

(37) Dash, S. R.; Rohani, S. Iterative Parameter Estimation for Extraction of Crystallization Kinetics of KCl from Batch Experiments. *Can. J. Chem. Eng.* **1993**, *71*, 539−548.
(38) Miller, S. M.; Rawlings, J. B. Model identification and control strategies for batch cooling crystallizers. *AIChE J.* **1994**, *40*, 1312−1327.

nucleation and growth kinetic parameters. The parameter vector of the nucleation and growth kinetics given in eqs 7 and 8 can be written in the form of:

$$\theta^T(t) = [k_b E_b b k_g E_g g] \tag{17}$$

Let us define the error as the difference between the measured, $y_{ij}(\theta)$, and the predicted, $\hat{y}_{ij}(\theta)$, values of a variable (e.g. the population density of a given size crystals) by:

$$e_{ij}(\theta) = y_{ij}(\theta) - \hat{y}_{ij}(\theta) \tag{18}$$

A least-squares parameter estimation requires minimization of the following objective function:

$$\min_{\theta} \phi(\theta) = \sum_{i=1}^{N_v} \sum_{j=1}^{N_m} e_{ij}^2(\theta) \tag{19}$$

subject to the crystallizer model equations

where N_v and N_m represent the number of variables and measurements, respectively. A weighted least-squares method is preferable if all measurements are not equally significant. If the weights to be assigned to each measurement are not known, a maximum likelihood estimation technique can be used to estimate the weights along with the parameter vector. The weights leading to a least-variance estimate are given by the elements of the inverse of the covariance matrix of the errors.[39] If all the errors are independent and distributed randomly with zero mean, the maximum likelihood method is equivalent to minimizing

$$\min_{\theta} \phi(\theta) = \sum_{i=1}^{N_v} \frac{N_i}{2} \ln\left(\sum_{j=1}^{N_m} e_{ij}^2(\theta)\right) \tag{20}$$

subject to the crystallizer model equations

and estimates of the elements of the covariance matrix are:

$$\hat{V}_{ii} = \frac{1}{N_{ij}} \sum_{j=1}^{N_m} e_{ij}^2(\theta) \tag{21}$$

II.3. Measurement of the Product Quality in Crystallization Processes. Recently there have been some successes for the real-time characterization of product quality in a crystallization process, namely measurement of supersaturation, crystal size distribution, product purity, product morphology, polymorphic distribution, and the product yield. There is often a distinction made between an inline and an online measurement of process variables. The former refers to the measurement inside the crystallizer (in situ), while the latter involves measurements of a sample that is diverted from the crystallizer. A noninvasive inline measurement is most desirable.

Apart from the conventional instrumentation to measure temperature, liquid level, suspension density, pressure and flow rate, other instrumentation is needed to measure the key process variables in a crystallization process. These include supersaturation, crystal size distribution, crystal morphology or habit, crystal purity, and polymorphic distribution of the product.

Supersaturation has been measured indirectly in terms of the solution density, refractive index, and solution thermal conductivity.[40] These methods are, however, often inaccurate and limited to two-component systems. Fourier transform infrared (FTIR) and Raman spectroscopy have been used[25−29] along with powerful chemometrics methods with relative success for the inline measurement of supersaturation. These methods require careful calibration and expensive instrumentation.

Inline *particle size measurement* has been the subject of great interest in the crystallization community. Forward and backscattering of laser light, focused beam reflectance measurement (FBRM), and ultrasound probes[41−43] have shown some success. The forward and backscattering of laser light instruments work in dilute slurries. The FBRM and the ultrasound probes work in higher slurry densities. The FBRM measures the chord length distribution of particles. Conversion of these measurements to particle size distribution (PSD), involves sophisticated mathematical algorithms.[44] Due to the problems involved in direct measurement of the PSD, Rohani and Paine[45] suggested an innovative fines suspension sensor (FSDS) that measures the solids concentration of crystals smaller than a cutoff size, e.g., 50 μm. The sensor was subsequently used in a series of trials[16−18,49,50] to control the CSD in batch and continuous crystallizers of different scales including a 1 m^3 pilot plant continuous crystallizer.

Crystal *habit* or *morphology* can be measured with the help of a camera and image analysis software. Hundal et al.[30] used Fourier descriptors to identify the shape of a population of KCl crystals, in an offline fashion. To classify the crystals into several shape classes, a supervised neural network was used. The technique was compared with the mathematical morphology algorithms and the principal component analysis for classification.[51,52] Recently, Mettler

(39) Bard, Y. *Nonlinear Parameter Estimation*; Academic Press: New York, 1974.

(40) Redman, T. P.; Rohani, S. On-line Determination of Supersaturation of a KCl-NaCl Aqueous Solution Based on Density Measurement. *Can. J. Chem. Eng.* **1994**, *71*, 64−71.

(41) See: http://www.lasentec.com.

(42) Mougin, P.; Wilkinson, D. In situ measurement of particle size during the crystallization of L-glutamic acid under two polymorphic forms: Influence of crystal habit on ultrasonic attenuation measurement. *Cryst. Growth Des.* **2002**, *2*, 227−234.

(43) Higgins, J. P.; Arrivo, S. M.; Thurau, G.; Green, R. L.; Bowen, W.; Lange, A.; Templeton, A. C.; Thomas, D. L.; Reed, R. A. Spectroscopic approach for on-line monitoring of particle size during processing pf pharmaceutical nanoparticles. *Anal. Chem.* **2003**, *75*, 1777−1785.

(44) Tadayyon, A.; Rohani, S. Determination of PSD by ParTec 100: Modeling and Experimental Results. *Part. Part. Syst. Charact.* **1998**, *15*, 127−135.

(45) Rohani, S. S.; Paine, K. Measurement of Solids Concentration of a Soluble Compound in a Saturated Slurry. *Can. J. Chem. Eng.* **1987**, *65*, 163−165.

(46) Palanki, S.; Krothapally, M. On-line optimization of batch processes. *Trends Chem. Eng.* **1998**, *5*, 45−69.

(47) Rohani, S.; Bourne, J. R. Simplified approach to the operation of a batch crystallizer. *CJChE*. **1990**, *68*, 795−806.

(48) Visser, E.; Srinivasan, B.; Palanki, S.; Bonvin, D. A feedback-based implementation scheme for batch process optimization. *J. Process Control*. **2000**, *10*, 399−410.

(49) Rohani, S.; Paine, K. Feedback Control of Crystal Size Distribution in a Continuous Cooling Crystallizer. *Can. J. Chem. Eng.* **1991**, *69*, 165−172.

(50) Redman, T.; Rohani, S.; Strathdee, G. Control of Crystal Mean Size in a Pilot Plant Potash Crystallizer. *I. Chem. E. Trans.* **1997**, *75*(A), 183−192.

(51) Bernard-Michel, B.; Rohani, S.; Pons, M. N.; Vivier, H.; Hundal, H. S. Classification of Crystal Shape Using Fourier Descriptors and Mathematical Morphology. *Part. Part. Syst. Charact.* **1997**, 14.

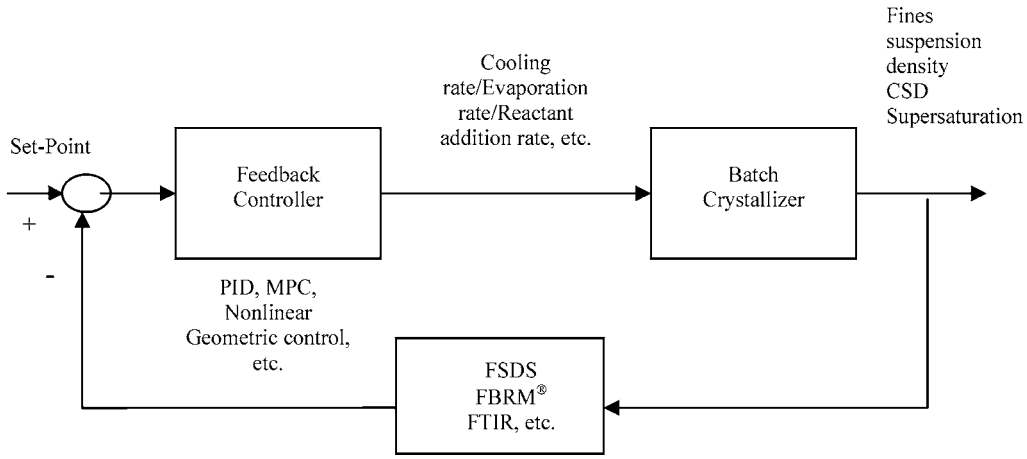

Figure 1. **Block diagram of a simple feedback controller for the direct/inferential control of product quality.**

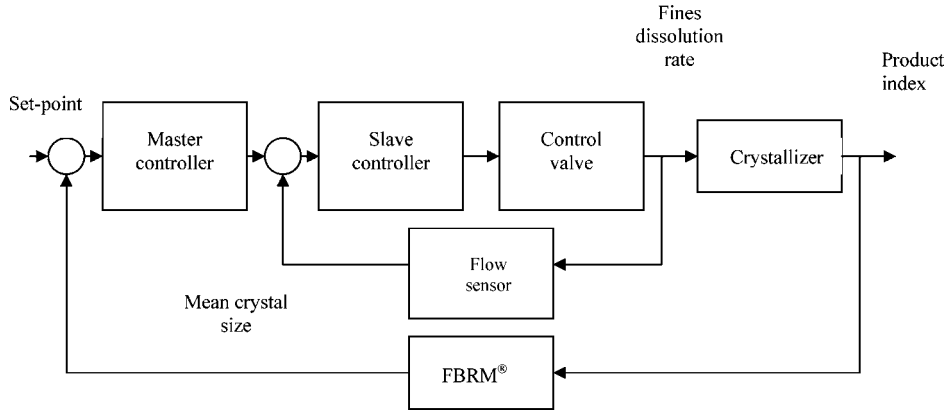

Figure 2. **Block diagram of a cascade feedback controller for the direct/inferential control of product quality.**

Toledo has introduced an image analyzer, PVM, for online monitoring of the crystal habit.[41]

Polymorphic distribution of pharmaceutical solids, fine chemicals, pigments, and food products may have significant effect on their physical properties. Various techniques such as the optical polarized thermomicroscopy, scanning electron microscopy (SEM), thermal analysis with the DSC (differential scanning calorimetry) and TGA (thermal gravimetric analysis), vibrational spectroscopy (such as solid-state FTIR, diffuse reflectance IR and Raman), single crystals and powder X-ray diffraction (XRD), and solid-state NMR are among analytical tools currently used for the characterization of polymorphism, albeit in an offline manner. The definitive analytical tool is single-crystal XRD. Recently, Raman and near-IR and high-energy XRD have been implemented for online monitoring of polymorphic transformation in a crystallizer.[53,54]

II.3. Direct/Inferential Feedback Control of Batch Crystallizers. If any of the major process variables in a crystallization process such as crystal size distribution, crystal morphology or polymorphic distribution of the product were available inline, an effective feedback controller could be designed for the control of the specific property that is being measured. In the absence of such measurement, control of supersaturation, the driving force of crystallization, often guarantees product quality. Figure 1 shows the closed-loop block diagram of such a feedback control system. The feedback controller can be a simple PID (proportional-integral-derivative) algorithm that, except for the tuning of its parameters, does not require an accurate model of the process, or the feedback controller can be a sophisticated model predictive controller or a geometric nonlinear controller.[20−24]

A limited number of experimental studies have been reported in the literature for the actual feedback control of crystal quality. To control the CSD, Rohani and his group[16−18,49,50] used the fines suspension density sensor (FSDS) to measure the fines concentration in a crystallizer. External or internal fines dissolution rate was used as the manipulated variable. The performance of the FSDS was shown to be superior to that of the FBRM in controlling the CSD, in a continuous crystallizer.[49,50] Figure 2 shows a cascade controller used in the CSD control of a pilot plant crystallizer.[50] In this configuration, if the crystallizer is a cooling type, the fines dissolution rate can be used as the manipulated variable. This may be achieved internally either by adding solvent or steam (if the solvent is water) in the

(52) Bernard-Michel, B.; Pons, M. N.; Vivier, H.; Rohani, S. The Study of Calcium Oxalate Precipitation Using Image Analysis. *Chem. Eng. J.* **1999**, *75*, 93−103.
(53) Anquetil, P. A.; Brenan, C. J. H.; Marcolli, C.; Hunter, I. W. Laser Raman spectroscopic analysis of polymorphic forms in microliter fluid volumes. *J. Pharm. Sci.* **2003**, *92*, 149−160.
(54) Blagden, N.; Davey, R.; Song, M.; Quayle, M.; Clark, S.; Taylor, D.; Nield, A. A novel batch cooling crystallizer for in-situ monitoring of solution crystallization using energy-dispersive X-ray diffraction. *Cryst. Growth Des.* **2003**, *3*, 197−201.

quiescent zone of the crystallizer where the concentration of fines is high, or by insertion of a ring-type heating element in the same region, and selectively dissolve the fines. Fines dissolution is more often carried out externally by diverting a suspension stream from the quiescent zone of the crystallizer, dissolving the fines by adding heat or solvent to the suspension, and returning the solution back to the crystallizer. Care must be exerted, however, to ensure that the solution is near saturation on its return to the crystallizer. If the returning solution is supersaturated or under-saturated, it may cause unwanted nucleation or dissolution. If antisolvent or reactive crystallization is used, the manipulated variable can be the rate of addition of the antisolvent or one of the reactants.

Matthews and Rawlings[5] used a turbidity sensor to measure the obscuration and, hence, controlled the CSD. Control of supersaturation using an online density meter[24] for FTIR and Raman spectroscopy has also been reported.[55,56] Control of crystal habit has been tried by Patience and Rawlings[31] using an inline image-capturing camera.

The major bottleneck in implementing the feedback controllers on crystallization processes is the lack of reliable inline measurement of the key process variables. As more accurate inline sensors become available, it is envisaged that the feedback controllers, as opposed to the optimal controllers, will be used more, due to their simplicity and lack of complete dependence on an accurate process model.

II.4. Optimal Control of Batch Crystallizers. To the best of our knowledge, the first attempt in implementing a type of optimal control policy on a batch crystallization process goes back to the work of Mullin and Nvylt.[1] They noticed that in a cooling batch crystallizer, a natural cooling policy (NCP) leads to a large peak in the supersaturation that leads to spontaneous nucleation and undesirable final CSD. A linear cooling policy (LCP) and a near optimal cooling policy, referred to as the controlled cooling policy (CCP), reduce the supersaturation peak and result in better (larger mean size and narrower size distribution) final CSD. In a seeded batch crystallizer, the possibility of ending up with a bimodal CSD, in the case of natural and linear cooling policies, is quite high. After that realization, a series of studies were conducted ranging from the simple extension of that work to the various crystallizing systems, to the design and implementation of sophisticated optimal control algorithms, as discussed in the Introduction.

Recently Hojjati and Rohani[57] conducted a thorough study on an ammonium sulfate−water cooling batch crystallizer. It was shown that, irrespective of the cooling policy, the size distribution of the final product can be made unimodal, provided that enough seeds are used (see Figures 3 and 4).

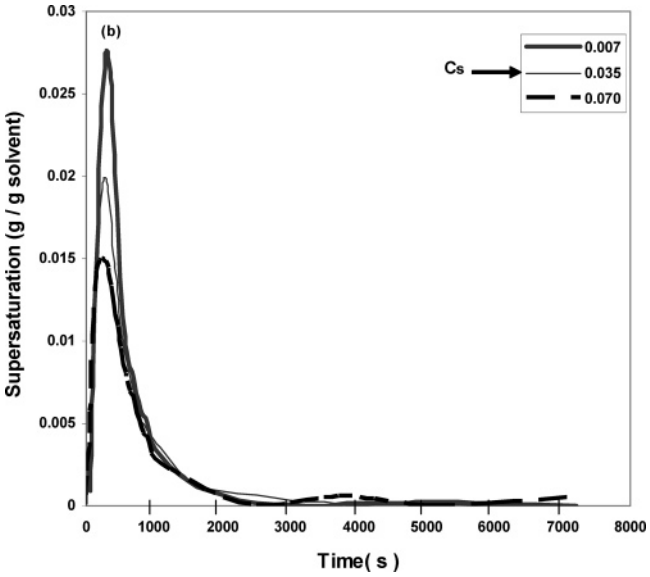

Figure 3. **Effect of seed loading on the supersaturation profile with a natural cooling policy and a mean seed size of 165 μm for ammonium sulfate−water system.**

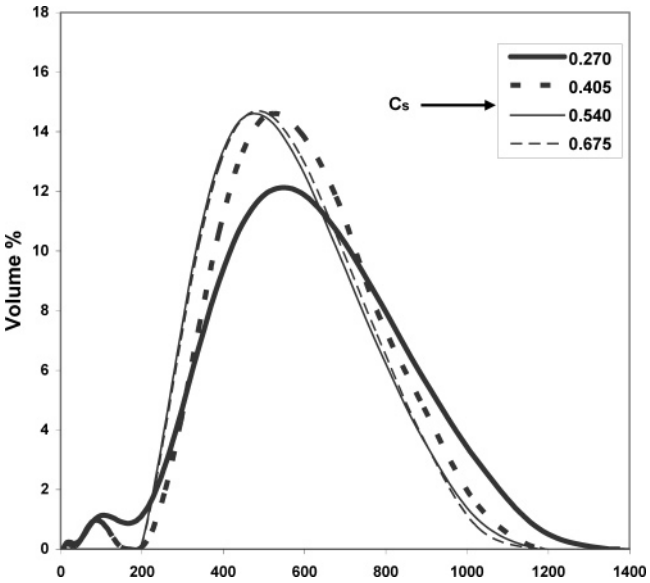

Figure 4. **Effect of seed loading on the final CSD with a natural cooling policy and a mean seed size of 165 μm for ammonium sulfate−water system.**

To obtain a product with a unimodal size distribution, however, the NCP needed more than 4 times of the amount of seeds compared to the CCP. Jagadesh et al.[58] and Hojjati and Rohani[57] used a seed chart, in which the dimensionless mean size ($L_{s,f}/L_s$) was plotted vs $(1 + C_s)/C_s$ along with the "ideal growth" curve, to present the effect of seeding policy on the final CSD. C_s is the normalized concentration of the seeds (seed loading), W_s/W_{theo}, where W_s is the mass of the seeds in kilograms and W_{theo} is the theoretical yield of crystals in kilograms. The "ideal growth" equation can be derived from a simple mass balance equation assuming no nucleation, no breakage, no agglomeration, and no change in the crystal shape.

(55) Fujiwara, M.; Chow, P. S.; Ma, D. L.; Braatz, R. D. Paracetamol crystallization using laser backscattering and ATR-FTIR spectroscopy: Metastability, agglomeration and control. *Cryst. Growth Des.* **2002**, *2*, 363−370.

(56) Starbuck, C.; Spartalis, A.; Wai, L.; Wang, J.; Fernandez, P.; Lindemann, C. M.; Zhou, G. X.; Ge, Z. Process optimization of a complex pharmaceutical polymorphic system via in-situ Raman spectroscopy. *Cryst. Growth Des.* **2002**, *2*, 515−522.

(57) Hojjati, H.; Rohani, S. Cooling and seeding effect on supersaturation and final crystal size distribution (CSD) of ammonium sulphate in a batch crystallizer. *Chem. Eng. Process.* **2004**. In print.

(58) Jagadesh, D.; Kubota, N.; Yokota, M.; Doki, N.; Sato, A.; Tavare, N. Large and Mono-Size Product Crystals from Natural Cooling Mode Batch Crystallization. *J. Chem. Eng. Jpn.* **1996**, *29*, 865−873.

$$\frac{L_{s,f}}{L_s} = \left(\frac{1 + C_s}{C_s}\right)^{1/3}$$

Figure 5 shows that for all cooling policies and seed mean sizes, increasing the seed loading pushes the $L_{s,f}/L_s$ curve closer to the "ideal growth" curve. The theoretical critical seed loading, $C^{theo}_{s,c}$, is defined as the seed loading at the intersection of the experimental curve and the ideal growth curve. With the help of the seed chart and the definition, $C^{theo}_{s,c}$, it has been shown that the seed loading higher than the $C^{theo}_{s,c}$ can improve the quality of the final CSD even if the NCP is used.[59] Figure 5 is plotted for all experiments performed in our laboratory in the ammonium sulfate−water cooling batch crystallizer with different seed sizes and under different cooling modes. For each seed size the $C^{theo}_{s,c}$ of all cooling modes is almost the same, but there is a remarkable difference between $C^{theo}_{s,c}$ and $C^{E}_{s,c}$, especially for the controlled cooling mode.

II.4.1. Open-Loop Optimal Control. As discussed in the Introduction, the interest in the control of batch crystallizers started by studying the programmed cooling of seeded and unseeded crystallizers. The crystallizer model including the mass and energy balances, with either the population balance or, more commonly, the moments equations, is used as the constraint to the optimization problem. The objective function is defined in terms of the CSD or a measure thereof, e.g. maximization of the final mean crystal size and/or minimization of the spread of the final CSD or the mass of the newly nucleated crystals.

Let us consider a seeded batch crystallizer model given by eqs 2−5 and assume that a rigorous parameter estimation procedure presented by eqs 19−21 has rendered reliable kinetic parameters given in eq 17. The rates of nucleation and growth kinetics given by eqs 7 and 8 provide the boundary condition for the solution of the population balance (eq 3). This information is needed in the optimization and subsequent implementation of the open-loop optimal control. A general statement of the optimal control is:

$$\min_{T(t)} \quad J = M_n(t_f) - M_s(t_f) \tag{22}$$

subject to the crystallizer model equations

where M_n and M_s are the mass of the newly nucleated and grown seed crystals, respectively, and t_f is the final batch time. This objective function minimizes the mass of the newly formed crystals in comparison with the grown seeds and results in a large mean crystal size at the end of the batch. The solution of eq 22 renders the optimal temperature profile that has to be followed to ensure the objective function J.

The seeded batch crystallizer given by Shi et al.[60] is considered here. The solubility concentration (C^*) and the limit of the metastable zone (C_m) are given by:

(59) Kubota, N.; Doki, N.; Yokota, M.; Sato, A. Seeding Policy in Cooling Crystallization. *Powder Technol.* **2001**, *121*, 31−38.

(60) Tavare, N. S.; Garside, J. Simultaneous estimation of crystal nucleation and growth kinetics from batch experiments. *Chem. Eng. Res. Des.* **1986**, *64*, 109−118.

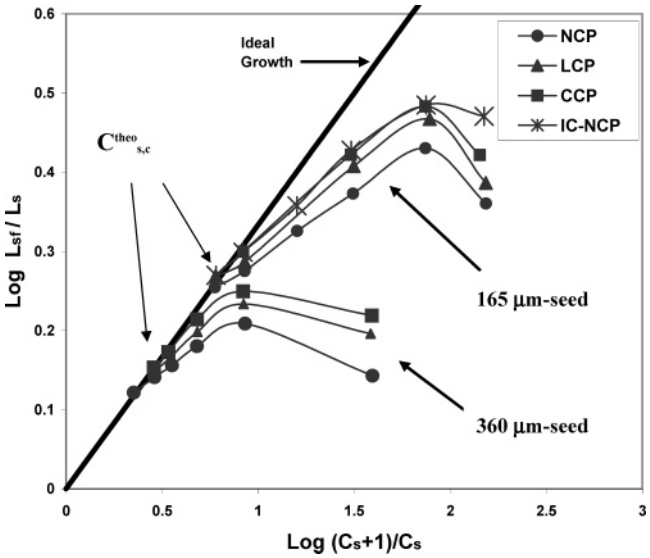

Figure 5. **Seed chart. At high seed loading all cooling policies approach the ideal growth with a unimodal product crystal size distribution.**

$$C^*(T) = [(6.29 \times 10^{-2}) + (2.46 \times 10^{-3})][T - (7.14 \times 10^{-6})]T^2 \tag{23}$$

$$C_m(T) = [(7.76 \times 10^{-2}) + (2.46 \times 10^{-3})][T - (8.10 \times 10^{-6})]T^2 \tag{24}$$

The initial seed distribution is assumed to be $n_s(r_s,0) = 0.0032(300 - r_s)(r_s - 250)$ for $250\ \mu m \le r_s \le 300\ \mu m$, and $n_s(r_s,0) = 0$ for $r_s < 250\ \mu m$ and for $r_s > 300\ \mu m$. The initial size domain was divided into 100 contiguous elements. The time step was set to 20 s. The initial solute concentration was 0.1743 g solute/g solvent. The parameter vector given in eq 17 was estimated, and the constrained optimization problem in eq 22 was solved. The energy balance was not needed since the temperature measurements were available. A sequential quadratic programming algorithm in Matlab was used. The constraints included 30 °C $\le T \le$ 50 °C, $C^* \le C \le C_m$, and $dT/dt \le 0$. Compared to a linear cooling profile 53% reduction in the mass of the newly generated nuclei was achieved using the optimal control policy.

II.4.2. Real-Time Optimal Control. The open-loop optimal controller, discussed above, is insensitive to changes that might occur during a batch operation or between one batch to another. To implement a real-time optimal control policy, the crystallizer model or the nucleation and growth parameters, or the system states have to be updated in an online fashion. Once the model, parameters of the model, or the system states are updated, the optimization problem recalculates the new optimal policy. The new optimal policy is implemented for the next time interval until the new updates become available.

Figure 6 shows the block diagram of a real-time optimal control system for a cooling batch crystallizer. For a closed-loop seeded potash alum batch crystallizer, eqs 13−15 are revised as follows:

$$\dot{x} = f(x) + g(x)u \tag{25}$$

where

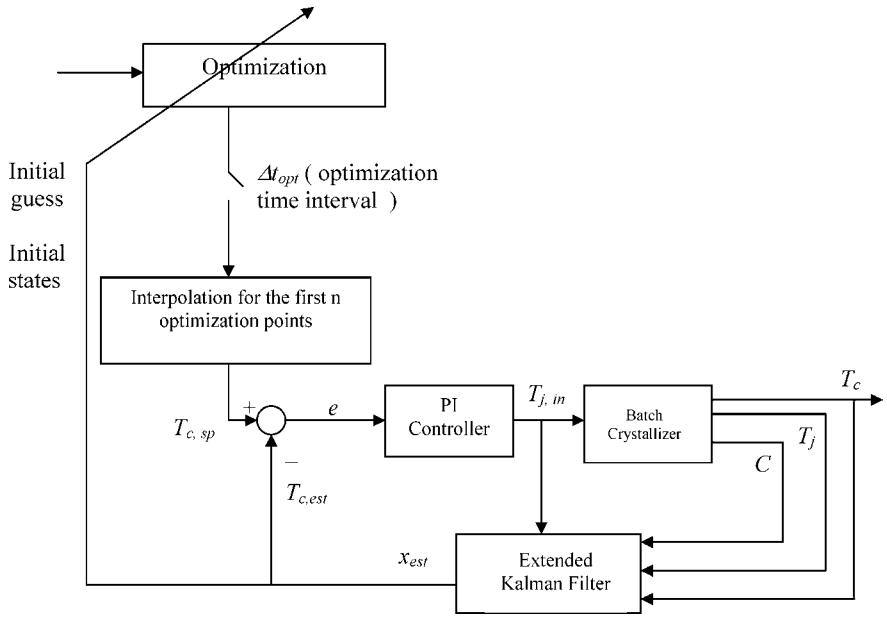

Figure 6. **Block diagram of the real-time optimal controller.**

$$x^T = [x_1 \cdots x_{10}]$$
$$= [m_{N,0} \cdots m_{N,5} C L_s T T_j] \tag{26}$$

$$f(x) = \begin{bmatrix} f_1(x) \\ \vdots \\ f_{10}(x) \end{bmatrix} = \begin{bmatrix} B \\ x_1 G \\ 2x_2 G \\ 3x_3 G \\ 4x_4 G \\ 5x_5 G \\ -3\rho_c k_v G(N_s x_8 + x_3) \\ G \\ \dfrac{-UA(x_9 - x_{10}) - 3W\Delta H \rho_c k_v G(N_s x_8{}^2 + x_3)}{W c_{pw}(1 + x_7) + W \rho_c k_v c_{pc}(N_s x_8{}^3 + x_4)} \\ -x_{10}\dfrac{F_w}{V_j} + \dfrac{UA}{\rho_w V_j c_{pw}}(x_9 - x_{10}) \end{bmatrix} \tag{27}$$

$$g^T(x) = \left[0 \cdots 0 \frac{F_w}{V_j}\right] \tag{28}$$

$$u = T_{j,in} \tag{29}$$

where x is the new state vector, $m_{N,0}$ to $m_{N,5}$ are the first six leading moments of the newly generated crystals, C is the solute concentration, L_s is the size of the seed crystals, T_c is the temperature inside the crystallizer, T_j is the cooling jacket temperature, and $T_{j,in}$ is the inlet cooling jacket temperature that is selected as the manipulated variable. The nucleation rate and the rate of crystal growth are reported by Tavare and Garside:[60]

$$G(t) = k_g N^{2.76} \Delta C(t)^{0.765} \tag{30}$$
$$B(t) = k_b \rho_c k_v (N_s x_8{}^3 + x_4) G^{1.88}$$

Table 1. **Operating conditions and physical parameters of the potash alum batch cooling crystallizer**

$T^*(0)$	45 °C	V_j	15 L
$T(0)$	40 °C	F_w	1 L/s
N	13.2 rev·s^{-1}	ρ_w	1000 kg/m^3
W	27 kg	ρ_c	1760 kg/m^3 crystal
UA	800 J/K·s	k_v	1
ΔH	44.5 kJ/kg crystal	$c_{p,w}$	3.8 kJ/K·kg solution
t_f	4800 s	$c_{p,c}$	0.84 kJ/K·kg crystal

where k_g and k_b are the growth and nucleation constants, N is the rotational speed of the stirrer, t is the time, N_s represents the total number of the seed crystals, and $\Delta C(t)$ is the supersaturation, which is defined by

$$\Delta C(t) = C[T(t)] - C^*[T(t)] \tag{31}$$

where $C^*[T(t)]$ is the equilibrium solute concentration at temperature T. Table 1 lists the physical parameters and the operating conditions of the crystallizer.

Since the crystallizer temperature, T, is the variable to be optimized and only the first eight states are required to calculate the objective function, the first eight state space equations form the equality constraints, and the bounds on the crystallizer temperature signify the inequality constraints of the optimization problem. Thus, the optimal control problem of the batch crystallization process can be stated as maximization of the weighted-mean size of the crystals and minimization of the coefficient of variation of the final CSD. The constant 0.0005 of CV is to assign similar significance to the mean size and the coefficient of variation of the final CSD.

$$\begin{aligned} \underset{T}{\text{nub}} \quad & J = -L_{wm}(t_f) + 0.0005 CV_{wm}(t_f) \\ \text{subject to:} \quad & [\dot{x}_1 \cdots \dot{x}_8]^T = [f_1(x) \cdots f_8(x)]^T \\ & 283\ \text{K} \le T \le 340\ \text{K} \end{aligned} \tag{32}$$

The optimal solution can approximately be represented by a set of discrete values of T: $T(0)$, $T(1)$, ..., $T(p)$, with the

optimization time interval Δt_{opt}. The set of ordinary differential equations in eq 25 is integrated, and the objective function, J, is evaluated at each optimization search iteration, j. The Runge−Kutta method was used to solve eq 25, and the Matlab function, *fmincon*, was used to solve the optimization problem.

Implementation of the online optimal control requires knowledge of the current states of the system. However, in practice, most of the states cannot be measured directly. An extended Kalman filter (EKF) was used to estimate the unmeasurable state variables every Δt_{opt}. The EKF involves a model-based update stage and a measurement-based update stage:

$$\dot{\hat{x}}(t) = f(\hat{x},t)$$
$$\hat{x}(0) = x_0 \tag{33}$$

$$\dot{P}(t) = F(\hat{x},t)P(t) + P(t)F^T(\hat{x},t) + Q(t)$$
$$P(0) = P_0 \tag{34}$$

where $\dot{x}$ and $\dot{P}$ represent the derivative of the estimated state vector and the error covariance matrix, respectively. Both of these are integrated in the sampling time interval from $l - 1$ to l to render the predictions of $\hat{x}_l(-)$ and $P(-)$. The initial state and the initial error covariance matrix are expressed as x_0 and P_0, and F is the Jacobian matrix of f defined by

$$F(\hat{x},t) = \left(\frac{\partial f}{\partial x}\right)_{x=\hat{x}} \tag{35}$$

Corrections for the estimations $\hat{x}_l(-)$ and $P(-)$ are computed by minimizing the estimation error. These corrected estimations are shown by $\hat{x}_l(+)$ and $P(+)$, respectively.

$$\hat{x}_l(+) = \hat{x}(-) + K_l[Z_l - h(\hat{x}(-))] \tag{36}$$

$$P_l(+) = [I - K_l H_l(\hat{x}_l(-))]P_l(-) \tag{37}$$

where H_l is the Jacobian matrix of h

$$H_l(\hat{x}_l(-)) = \left(\frac{\partial h}{\partial x}\right)_{x=\hat{x}}(-) \tag{38}$$

and K_l is the Kalman gain matrix, which can be calculated by

$$K_l = P_l(-)H_l^T(\hat{x}_l(-))[H_l(\hat{x}_l(-))P_l(-)H_l^T(\hat{x}_l(-)) + R_l]^{-1} \tag{39}$$

At each integration step, the EKF calculates the model-based state estimates (eq 33) and the model-based state error covariance (eq 34) by using the fourth-order Runge−Kutta method. Then, based on the new available measurements, corrections of the new predictions are made using eqs 36 and 37.

Figure 7 compares the cooling profiles obtained from a simplified cooling policy proposed in ref 4 and the optimal cooling policy presented in this work. Figures 8 and 9 compare the nucleation and growth rates obtained by these two cooling policies. Figures 7 and 10 show the ability of the extended Kalman filter to estimate the crystallizer temperature, solute concentration, and the jacket temperature,

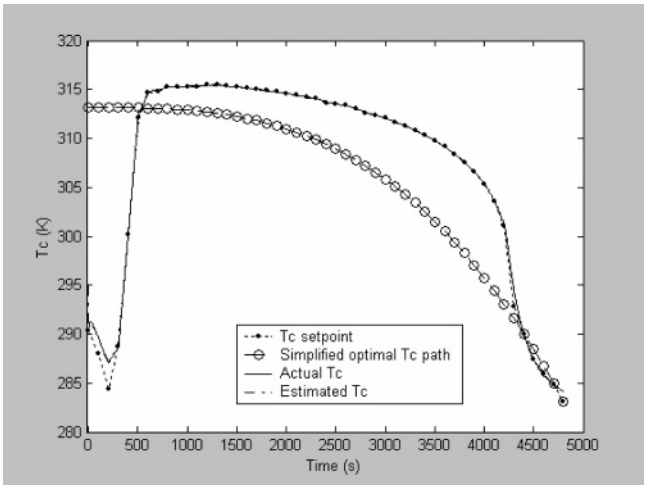

Figure 7. **Comparison of the cooling profiles obtained by the optimal and the simplified (a third-order polynomial) policies.**

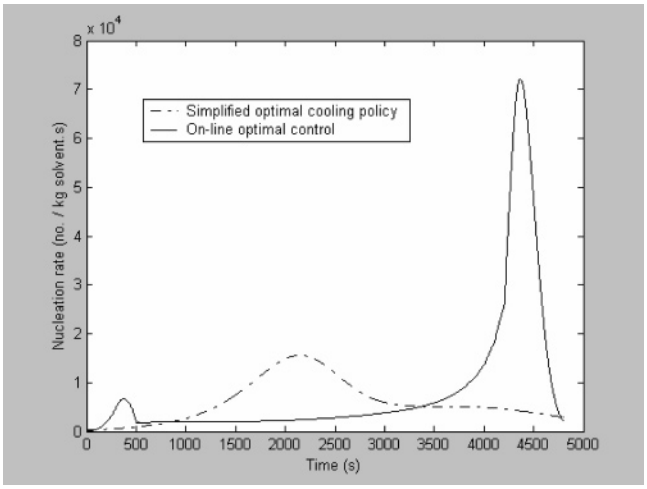

Figure 8. **Nucleation rate profile using the optimal and the simplified cooling policies.**

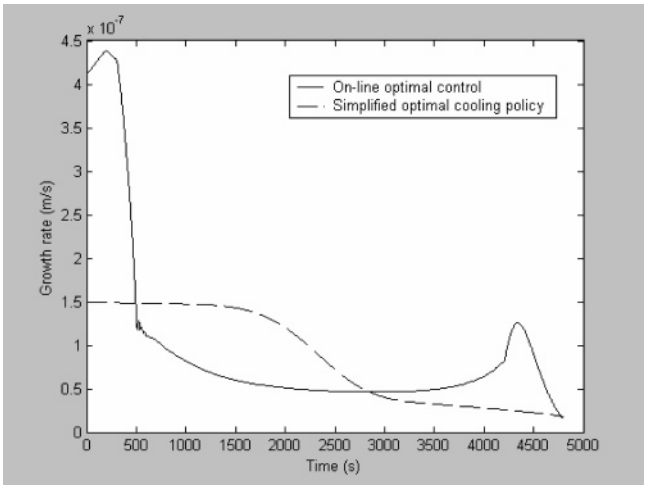

Figure 9. **Growth rate profile using the optimal and the simplified cooling policies.**

respectively. Table 2 shows that the online optimal control improves the final product quality by increasing the final weight mean size from 269×10^{-6} m to 303×10^{-6} m, and decreasing the coefficient of variation of the final CSD from 0.462 to 0.370, in comparison to a simplified optimal cooling

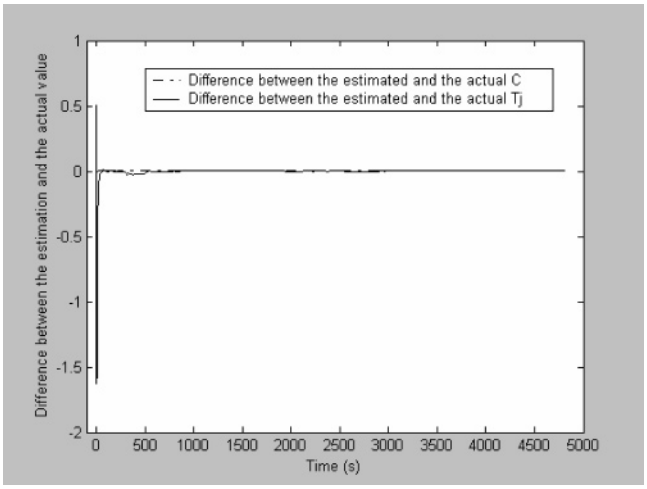

Figure 10. **Comparison of the estimated (by the extended Kalman filter) and calculated (actual) solute concentration and the jacket temperature.**

Table 2. **Comparison of the final product CSD of the batch crystallizer in the ideal case (perfect model with no disturbances)**

operating policy in the ideal case	L_{wm} (10^{-6} m)	CV_{wm}
simplified optimal cooling	269	0.462
online optimal control cooling	303	0.370

Table 3. **Testing the real-time optimal control strategy in the presence of model/plant mismatch and the comparison with the off-line simplified optimization**

		L_{wm} (10^{-6} m)		CV_{wm}	
case	mismatch	real-time	offline	real-time	offline
(a)	$k_{b,\,actual} = 1.2\,k_{b,\,model}$ $k_{g,\,actual} = 0.9k_{g,\,model}$	294	293	0.380	0.369
(b)	$k_{b,\,actual} = 1.3\,k_{b,\,model}$ $k_{g,\,actual} = 0.8\,k_{g,\,model}$	289	287	0.411	0.429
(c)	$k_{b,\,actual} = 1.5\,k_{b,\,model}$ $k_{g,\,actual} = 0.8\,k_{g,\,model}$	285	282	0.422	0.430

policy.[4] To demonstrate the efficacy of the proposed real-time optimal controller, it was assumed that there are uncertainties associated with the nucleation and growth kinetic parameters. Table 3 shows three cases. In case (a), +20% error in the nucleation rate coefficient k_b, and −10% error in the growth rate coefficient k_g were assumed. In cases (b) and (c), there were +30%, −20% and +50%, −20% errors in k_b, k_g and k_g, and in k_b, respectively. It is observed that the online optimal control policy gives a good performance in terms of the quality of the final product despite the errors in k_b and k_g.

Alternative real-time optimal controllers of batch crystallizers have also been proposed by other researchers. For example, Chiu and Christofides[61,62] have proposed a nonlinear control algorithm for the real-time optimal control of chemical processes. In addition, the efficient algorithm for the solution of the population balance equation, presented in eq 11 coupled with the online kinetic parameter estimation, could offer an effective means for the implementation of real-time optimal controllers for batch crystallizers.

III. Conclusions

Most of the optimal (open-loop and real-time) control studies have been restricted to cooling batch crystallizers. The proposed algorithms, however, can be extended to other types of crystallization processes and for the control of all product quality indexes. The majority of industrially important crystallization processes are reactive or drowning-out type crystallizers. It is important that future studies address multivariable real-time optimal control systems in which simultaneous optimal cooling profile with the optimal reactant/antisolvent addition rate are sought. Implementation of a real-time multivariable optimal controller will certainly benefit from the algorithm for the solution of the population balance equation, presented in this work. Reliable sensors to measure important process variables such as the supersaturation, the size distribution of fine crystals, and polymorphic characterization will facilitate implementation of both feedback controllers and real-time optimal controllers on batch crystallizers.

Received for review March 28, 2005.

OP050050U

(61) Chiu, T.; Christofides, P. D. Nonlinear control of particulate processes. *AIChE J.* **1999**, *45*, 1279−1297.

(62) Liotta, V.; Sabesan, V. Monitoring and feedback control of supersaturation using ATR-FTIR to produce an active pharmaceutical ingredient of a desirable crystal size distribution. *Org. Process Res. Dev.* **2004**, *8*, 488−498.